

MIT Open Access Articles

High-resolution imaging of cellular dopamine efflux using a fluorescent nanosensor array

The MIT Faculty has made this article openly available. **Please share** how this access benefits you. Your story matters.

Citation: Kruss, Sebastian et al. "High-Resolution Imaging of Cellular Dopamine Efflux Using a Fluorescent Nanosensor Array." *Proceedings of the National Academy of Sciences* 114, 8 (February 2017): 1789–1794 © 2017 National Academy of Sciences

As Published: <http://dx.doi.org/10.1073/pnas.1613541114>

Publisher: National Academy of Sciences (U.S.)

Persistent URL: <http://hdl.handle.net/1721.1/111216>

Version: Final published version: final published article, as it appeared in a journal, conference proceedings, or other formally published context

Terms of Use: Article is made available in accordance with the publisher's policy and may be subject to US copyright law. Please refer to the publisher's site for terms of use.



High-resolution imaging of cellular dopamine efflux using a fluorescent nanosensor array

Sebastian Kruss^{a,1}, Daniel P. Salem^a, Lela Vuković^{b,c,2}, Barbara Lima^a, Emma Vander Ende^a, Edward S. Boyden^{d,e}, and Michael S. Strano^{a,3}

^aDepartment of Chemical Engineering, Massachusetts Institute of Technology, Cambridge, MA 02139; ^bDepartment of Physics, University of Illinois at Urbana–Champaign, Champaign, IL 61801; ^cDepartment of Chemistry, University of Texas at El Paso, El Paso, TX 79968; ^dMedia Lab, Massachusetts Institute of Technology, Cambridge, MA 02139; and ^eMcGovern Institute for Brain Research, Massachusetts Institute of Technology, Cambridge, MA 02139

Edited by David R. Walt, Tufts University, Medford, MA, and accepted by Editorial Board Member John A. Rogers January 11, 2017 (received for review August 23, 2016)

Intercellular communication via chemical signaling proceeds with both spatial and temporal components, but analytical tools, such as microfabricated electrodes, have been limited to just a few probes per cell. In this work, we use a nonphotobleaching fluorescent nanosensor array based on single-walled carbon nanotubes (SWCNTs) rendered selective to dopamine to study its release from PC12 neuroprogenitor cells at a resolution exceeding 20,000 sensors per cell. This allows the spatial and temporal dynamics of dopamine release, following K⁺ stimulation, to be measured at exceedingly high resolution. We observe localized, unlabeled release sites of dopamine spanning 100 ms to seconds that correlate with protrusions but not predominately the positive curvature associated with the tips of cellular protrusions as intuitively expected. The results illustrate how directionality of chemical signaling is shaped by membrane morphology, and highlight the advantages of nanosensor arrays that can provide high spatial and temporal resolution of chemical signaling.

sensors | imaging | dopamine | carbon nanotubes | chemical signaling

Chemical signaling between cells is a hallmark of life, with one key example being neurotransmitter release from neurons to transmit and process information (1). However, unlike electrical potential, the measurement of chemical signaling between cells and within cellular networks is not as well developed, despite its importance to cellular biology. Neurotransmission via neurotransmitters, paracrine signaling between immune cells, or quorum sensing between bacteria in biofilms (2, 3) rely on spatial and temporal precision in chemical signaling. Analytical tools are not yet available to resolve these dynamics. Recently, the groups of Lindau and Ewing used 4–16 microelectrodes per array per chromaffin cell to estimate catecholamine release direction and dynamics (4–6). Nanosensors have several advantages for the study of cell signaling, as we have highlighted (7, 8). Their nanoscale size means that they can form dense arrays, increasing the number of probes per cell. In this work, we construct a fluorescent nanosensor array placed in the vicinity of PC12 neuroprogenitor cells at a density of ~20,000 sensors per cell, with better than 100-ms temporal resolution to study dopamine release with much higher resolution.

The platform uses near-infrared (nIR) fluorescent single-walled carbon nanotubes (SWCNTs) rendered chemically selective to dopamine. nIR fluorescent single SWCNTs are versatile building blocks for biosensors and demonstrate detection limits down to single molecules (9–13). We selected the neurotransmitter dopamine for this study because of its central role for reward control and learning and because it is one of the neurotransmitters for which volume transmission is heavily discussed (14, 15). The spatially dependent concentration profile of dopamine plays an especially important role when neurotransmitters spill over from synapses and freely diffuse in all directions (volume transmission) through neural tissue (14, 16, 17). By placing such dopamine-sensitive nanosensors in arrays beneath dopaminergic cells we are able to image dopamine efflux, identify hotspots on the cell surface, and

map the directionality of dopamine efflux (Fig. 1A). This platform has advantages over protein-based fluorescent sensors and semi-synthetic protein–fluorophore conjugates on the cell surface in that it has higher sensitivity, time resolution, and lacks photobleaching (18–21). Electrochemical techniques, although the most advanced for measurement of redox-active neurotransmitters *in vitro* and *in vivo*, provide poor spatial resolution (4, 6) to date. Indirect (optical) methods can label cellular components that are involved in exocytosis or load vesicles with fluorescent dyes but cannot directly detect the molecules of interest or their dynamics in the extracellular space (22–24).

Results and Discussion

Previously we found that the corona phase around SWCNTs can be engineered to recognize certain small analytes—a phenomenon we termed Corona Phase Molecular Recognition (CoPhMoRe) (7, 25, 26). Specifically, DNA-wrapped SWCNTs were found to increase their nIR fluorescence in the presence of catecholamines (13). Here, we synthesized and characterized different DNA/SWCNT complexes and identified the best candidates for dopamine detection (*SI Appendix, Fig. S1*). We measured the fluorescence responses of a panel of 10 DNA-wrapped (6, 5)-chirality enriched SWCNTs versus a panel of 15 molecules (*SI Appendix, Figs. S2–S4*) including dopamine, dopamine homologs, and potential interfering compounds present in biological environments (*SI Appendix, Fig. S2*). Our results

Significance

Cells communicate between themselves using waves of chemical concentration that change in both direction and time. Existing methods are not able to capture this spatial and temporal dependence at the necessary resolution to study the influence of cellular morphology. This study utilizes arrays of fluorescent nanosensors based on single-walled carbon nanotubes placed under and around neuroprogenitor cells to label-free image the efflux of the neurotransmitter dopamine. We use the spatio-temporal resolution of this approach to resolve where on the cell surface dopamine is released and how cell morphology affects the location of release sites.

Author contributions: S.K., E.S.B., and M.S.S. designed research; S.K., D.P.S., L.V., B.L., and E.V.E. performed research; S.K., D.P.S., L.V., and M.S.S. analyzed data; and S.K., D.P.S., and M.S.S. wrote the paper.

The authors declare no conflict of interest.

This article is a PNAS Direct Submission. D.R.W. is a Guest Editor invited by the Editorial Board.

¹Present address: Department of Chemistry, Institute of Physical Chemistry, Göttingen University & Center for Nanoscale Microscopy and Molecular Physiology of the Brain, 37077 Goettingen, Germany.

²Present address: Department of Chemistry, University of Texas at El Paso, El Paso, TX 79968.

³To whom correspondence should be addressed. Email: strano@mit.edu.

This article contains supporting information online at www.pnas.org/lookup/suppl/doi:10.1073/pnas.1613541114/-DCSupplemental.

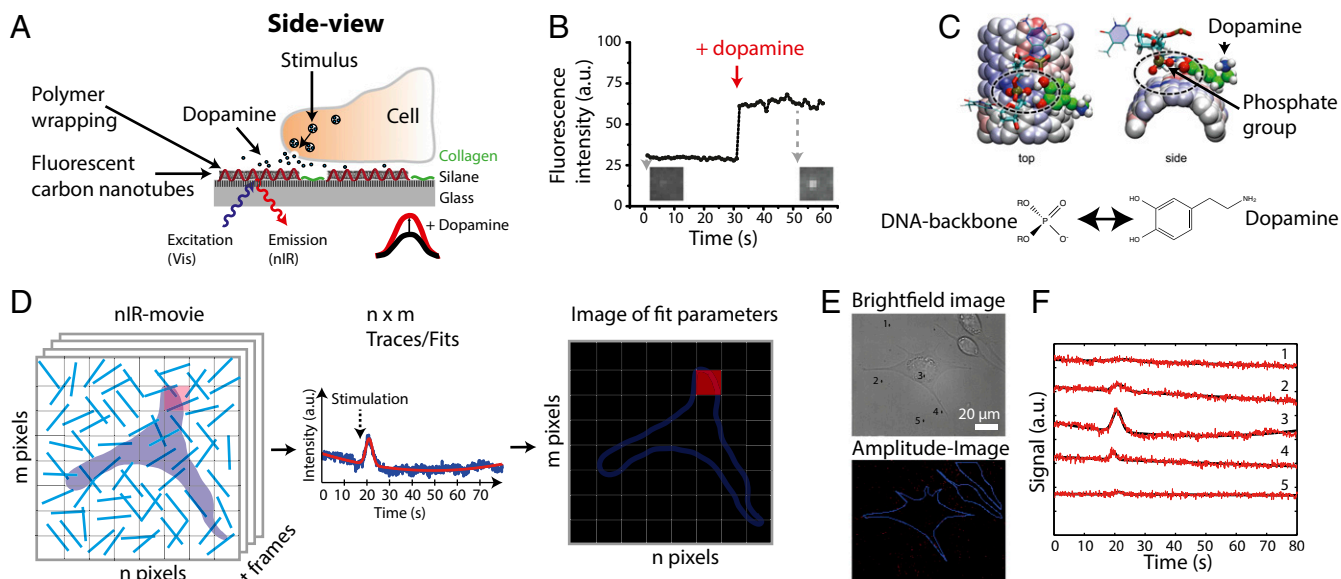


Fig. 1. Chemical imaging using nanosensor arrays. (A) Fluorescent carbon nanotubes are rendered sensitive to dopamine by noncovalently attaching specific DNA sequences to them. They are immobilized onto a glass substrate, and dopamine-releasing PC12 cells are cultivated on top. When cells are stimulated they release dopamine and the SWCNT fluorescence changes. (B) Fluorescence intensity trace of a single (GA)₁₅-ssDNA/SWCNT imaged on a surface while adding dopamine (10 μ M). (C) Proposed sensing mechanism: Dopamine pulls phosphate groups to the SWCNT surface, which removes quenching sites and increases SWCNT fluorescence quantum yield (MD simulations). (D) PC12 cells are cultivated on top of a substrate coated with nanosensors. In an image of this substrate every pixel corresponds to a region containing one or more nanosensors and serves as a reporter of local dopamine concentration. Each pixel of an nIR-movie produces a trace that contains information about the dopamine signal. A fitting procedure of every trace yields amplitude, width, and time point of the signal. Those values can be represented in false-color images, and their spatial composition can be further analyzed. (E) Bright-field image of a PC12 cell adhering on top of a nanosensor array and corresponding image of signal amplitudes. (F) Examples for pixel traces from regions under and around the cell shown in E.

indicate that (GA)₁₅-ssDNA/SWCNT complexes provide the most promising selectivity and sensitivity profile for cell experiments (Fig. 1B and *SI Appendix*, Figs. S4–S6). These dopamine nanosensors were excited with a laser at 560 nm in a standard fluorescence microscope equipped with an nIR-camera that detects the nIR emission of (6, 5)-SWCNTs at \sim 980 nm. We performed molecular dynamics (MD) simulations to gain a deeper understanding of molecular recognition of these sensors. Our results show that dopamine interacts via its two hydroxy groups with phosphate groups of the DNA backbone (Fig. 1C). This interaction pulls the phosphate group closer to the surface of the SWCNTs and changes the local potential (*SI Appendix*, Figs. S21–S26). These findings rationalize previous phenomenological theories of molecular recognition in the corona phase of SWCNTs (27, 28). Furthermore, we found that naked SWCNTs do not respond to dopamine at all (*SI Appendix*, Fig. S8 and S10) and the least responsive DNA sequences showed the highest (starting) fluorescence counts (*SI Appendix*, Figs. S9–S11). This result suggests that movement of the phosphate groups removes (pre-)quenching sites for excitons and that dopamine's ability to pull these groups to the SWCNT surface results in an increase of SWCNT fluorescence.

With respect to the envisioned application (Fig. 1A) we prepared homogeneously coated nanosensor surfaces and treated every pixel of the nIR image as a local sensor. Whereas nanosensors are randomly adsorbed on the surface, it would be possible to pattern them more regularly as it was shown for other nanoparticles (29–31). The SWCNT sensors were densely coated on the surface to maximize the signal/noise ratio (*SI Appendix*, Figs. S12–S14). Ensemble calibration curves (*SI Appendix*, Fig. S5) indicate that we can detect dopamine concentrations down to 100 nM (*SI Appendix*, Fig. S5). However, this is the mean response of a large population of sensors. When we analyzed individual nanosensors in the single-molecule regime (100 pM) we observed stochasticity indicative of binding and unbinding events of single dopamine

molecules (*SI Appendix*, Fig. S7). To ensure that our sensors were capable of detecting dopamine in the presence of cells, we cultivated dopamine-releasing pheochromocytoma cells (PC12) on top of nanosensor arrays that were additionally coated with collagen to increase cell adhesion (*SI Appendix*, Figs. S13–S16). Collagen has been known to increase PC12 cell adhesion and differentiation, whereas nanotubes affect neurite outgrowth (32–35). Furthermore, the elasticity of the substrate affects PC12 cell morphology (36). PC12 cells on our sensor/collagen-coated surfaces attained a morphology similar to PC12 cells cultured without sensors. Similar scenarios in the literature are nanotube networks that were glycosylated to enhance biocompatibility and have been used for amperometric studies of dopamine release (37). This procedure increased adhesion and viability of PC12 cells on SWCNT networks. We focused our investigation mostly on isolated PC12 cells and not clusters to minimize cross-talk from different cells.

Labeling with the fluorescent false neurotransmitter FFN551 showed that PC12 cells on these surfaces contain vesicles with dopamine transporters, indicating dopamine-containing vesicles (*SI Appendix*, Fig. S16) (24, 38). After 1 d of cultivation at 37 $^{\circ}$ C in full culture medium, the medium was exchanged to PBS buffer and the response to dopamine and homologs (10 μ M) was tested. The results (*SI Appendix*, Fig. S6) show that the nanosensor arrays are still functional and resist biofouling. Catecholamine homologs such as epinephrine, norepinephrine, and ascorbic acid could interfere with this array (*SI Appendix*, Fig. S6). Therefore, the sensor array reports about the total changes in the concentration of all catecholamines (ascorbic acid concentrations should be negligible/constant). However, PC12 cells are thought to mainly release dopamine even though pharmaceuticals and hypoxia can affect the ratio between the different catecholamine neurotransmitters (32, 39, 40). Consequently, sensor responses are expected to be attributed mainly to dopamine and to a lesser extent other catecholamines.

The results from Fig. 1 indicate that we can use surface-immobilized nanosensors to optically detect dopamine in the presence of PC12 cells. Consequently, we recorded nIR movies (100 ms per image, 640×512 -pixel resolution, 212 nm/pixel) of PC12 cells adhered on collagen-coated nanosensor arrays and stimulated the cells with potassium buffer to observe dopamine release. To increase the signal to noise ratio, we divided the field of view into squares of 4×4 pixels and developed a fitting algorithm for the normalized intensity traces of the pixel groups. This algorithm fits the curve $f(t) = a + bt + ct^2 + xe^{-(t-y)^2/2z^2}$ to the intensity traces (Gaussian function plus background correction; Fig. 1 D–F).

Consequently we get 20,480 “reporter” pixels per fitted image (pixel size $\sim 850 \times 850$ nm). Therefore, we expect $\sim 1,700$ reporter pixels under a (round) cell ($d = 40 \mu\text{m}$), >180 reporter pixels in a $2\text{-}\mu\text{m}$ zone around the cell, and ~ 150 reporter pixels under the cell contour (pixel size = 850×850 nm). The fitting process reduced the 3D movie to a 2D image of fitting parameters, which can then be further analyzed (Fig. 1D). The different fitting parameters represent how the local reporter pixel responds to dopamine and the parameters account for amplitude (x), width (y), and time point (z) of the event. Fig. 1F shows typical traces from different locations under the cell, from the cell border, and other regions [1–5, shown in the bright-field (BF) image of Fig. 1E].

We performed independent analyses to verify that (i) temporal and (ii) spatial patterns are related to the stimulation time point and the location of cells. To verify the temporal correlation in raw data traces (Fig. 2A), we defined three periods (before, during, and after stimulation) and searched for maxima (in each period) that would indicate a dopamine-induced fluorescence increase. The exact stimulation time point (± 1 s) was known from the time point when K^+ was added on top of the cells. The nonrandom distribution during the stimulation period proves that the observed sensor responses are related to stimulation (Fig. 2A and B).

Histograms of the normalized sensor signals from different regions of interest related to the cell (shown in white in Fig. 2C, Left) prove that the signals are not randomly distributed

throughout the image. Specifically, there is a clear spatial correlation between responses (normalized amplitude change) and regions associated with the cell (e.g., cell border, cell body). The time resolution of our approach (100 ms) is not yet fine enough to observe a propagating wave of dopamine released by the cell given that the diffusion length scale during image acquisition $x = \sqrt{2Dt}$ is $\sim 12 \mu\text{m}$ [$D = 7.63 \times 10^{-6} \text{cm}^2/\text{s}$ (14)], comparable to the cell diameter. However, the technique is able to localize release events and their duration as shown below.

Fig. 3A shows the fitted response of the sensors at different time points from the contour of a single cell (shown in Fig. 3B, Left). The 3D plots show the sensors turn on after cell stimulation, which indicates release of dopamine. Furthermore, the responses decay as dopamine unbinds and diffuses away. Fig. 3 B–E shows bright-field images of four different cells and corresponding 3D plots of the sensor response magnitudes along the cell contour (line width = 850 nm). Here, in contrast to the time-resolved Fig. 3A, the maximum responses of the whole experiment are shown (fit parameter x). The height and color of the 3D plots indicate the magnitude of sensor responses indicative of higher transient dopamine concentrations (Fig. 1D). For clarity we only show responses along this contour (full response plots are shown in *SI Appendix*, Fig. S17 and a time-resolved full hotspot analysis in *SI Appendix*, Fig. S18).

The contour is also the most interesting region because efflux parallel to the nanosensor array is centered there with dopamine concentrations highest at exocytosis sites. The response profiles show heterogeneity along the contour, which is expected from multiple dopamine release sites. Furthermore the shape of the cell affects the distribution of release sites. Fig. 3 demonstrates the superior spatial resolution of our sensing strategy compared with existing technology. For example, the groups of Lindau and Ewing used microelectrode arrays with up to 4–16 electrodes (per cell) to “image” catecholamine release from chromaffine cells (4–6). In contrast, our approach contains 349, 242, 192, and 206 sensor pixels just along the contour of the four cells shown in

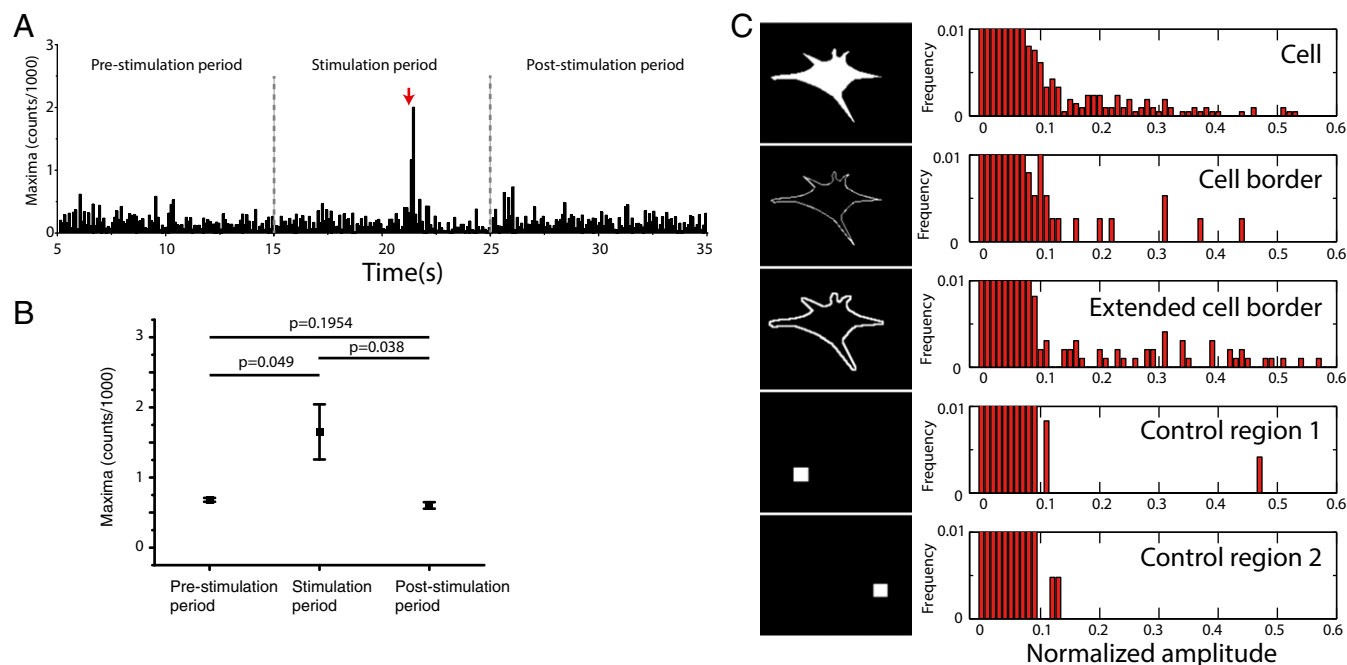


Fig. 2. Spatial and temporal correlation between sensor response and cells. (A) Temporal correlation between stimulation event and sensor responses (single experiment). (B) Large amplitudes are more likely in time intervals with cell stimulation. Two-sided t test of independent experiments ($n = 4$). (C) Spatial correlation between sensor responses (normalized amplitude change) and parts of the cell. The black/white image on the left indicates the regions/pixels (in white) that were analyzed. The histograms show that the sensor responses are related to the cell and are not randomly distributed.

Sensor surfaces were prepared by the following procedure. First, glass substrates (#1, ThermoScientific) were functionalized with (3-aminopropyl)triethoxysilane (APTES) in ethanol (1% APTES, 1% water, 1 h). Then DNA-wrapped SWCNTs [(GA)₁₅ ssDNA if not stated otherwise] were diluted 1:100 in PBS [corresponding to a final absorption of 0.0075 at the (6, 5)-SWCNT S₂₂-peak maximum at around 570 nm] and incubated on top of those surfaces to let them adsorb (1 h). Afterward these surfaces were rinsed 3× with PBS. Then they were incubated with a collagen solution (Collagen, Type I, C3867, Sigma) overnight at 4 °C and rinsed with PBS. For most experiments the glass substrates were mounted from the beginning in a flow chamber (ibidi sticky-Slide VI 0.4).

Finally, PC12 cells were sparsely cultivated in full medium on these surfaces to avoid clustering (at least 4 h). Cell adhesion was verified by light microscopy and the full medium was exchanged to PBS supplemented with calcium and magnesium (Sigma). Cells in the flow chamber and all buffers were kept at 37 °C before the experiment. Cell experiments were performed without an incubation chamber but given the time scale of the experiment (<10 min) the temperature was close to 37 °C. Cells were stimulated by adding 110 mM potassium chloride solution to the inlet of the flow chamber (final concentration ~55 mM for the complete flow chamber volume).

Data Analysis and Fitting Algorithm. Movies collected during cell experiments were processed by a fitting algorithm to identify regions where sensors responded to dopamine release. During each frame, the image of 640 × 512 pixels was separated into 4 × 4-pixel groups over which mean intensity values

were calculated, resulting in a time-dependent intensity trace for each of the 20,480 groups. Each intensity trace was fit to the following equation:

$$I = a + b \cdot t + c \cdot t^2 + x \cdot e^{(-(t-y)^2)/z^2}.$$

The functions formed by parameters *a*, *b*, and *c* represent the possible drift in baseline intensity caused by defocusing of the microscope during the experiment. The parameters *x*, *y*, and *z* represent the amplitude, peak center, and SD, respectively, of a Gaussian function used to fit a region of sensor response. A script was used to process the movies and perform the fittings. The fitting procedure provided images of fitting parameters.

The curvature of the cell contour was calculated by using a three-point approximation (48). For each pixel of the contour the mean (curvature) of the local pixel curvature plus three adjacent pixels was calculated.

ACKNOWLEDGMENTS. We thank Klaus Schulten and Markita Landry for input and support. S.K. was supported by the Deutsche Forschungsgemeinschaft and a Liebig Fellowship (Fonds der chemischen Industrie). D.P.S. is grateful for a National Science Foundation (NSF) Graduate Research Fellowship under Grant 2388357. L.V. was supported by NSF Grant PHY1430124 and NIH Grant 9P41GM104601. The authors acknowledge the NSF-funded Extreme Science and Engineering Discovery Environment CA935028, the Taub computing cluster (University of Illinois), and the Texas Advanced Computing Center for computational resources. Additional funding was provided by the McGovern Institute Neurotechnology Program.

- Hyman SE (2005) Neurotransmitters. *Curr Biol* 15(5):R154–R158.
- Thurley K, Gerecht D, Friedmann E, Höfer T (2015) Three-dimensional gradients of cytokine signaling between T cells. *PLoS Comput Biol* 11(4):e1004206.
- Camilli A, Bassler BL (2006) Bacterial small-molecule signaling pathways. *Science* 311(5764):1113–1116.
- Hafez I, et al. (2005) Electrochemical imaging of fusion pore openings by electrochemical detector arrays. *Proc Natl Acad Sci USA* 102(39):13879–13884.
- Wang J, Trouillon R, Lin Y, Svensson MI, Ewing AG (2013) Individually addressable thin-film ultramicroelectrode array for spatial measurements of single vesicle release. *Anal Chem* 85(11):5600–5608.
- Wang J, Ewing AG (2014) Simultaneous study of subcellular exocytosis with individually addressable multiple microelectrodes. *Analyst (Lond)* 139(13):3290–3295.
- Kruss S, et al. (2013) Carbon nanotubes as optical biomedical sensors. *Adv Drug Deliv Rev* 65(15):1933–1950.
- Polo E, Kruss S (2016) Nanosensors for neurotransmitters. *Anal Bioanal Chem* 408(11):2727–2741.
- Zhang J, et al. (2011) Single molecule detection of nitric oxide enabled by d(AT)₁₅ DNA adsorbed to near infrared fluorescent single-walled carbon nanotubes. *J Am Chem Soc* 133(3):567–581.
- Reuel NF, et al. (2013) Emergent properties of nanosensor arrays: Applications for monitoring IgG affinity distributions, weakly affined hypermannosylation, and colony selection for biomanufacturing. *ACS Nano* 7(9):7472–7482.
- Zhang J, et al. (2014) A rapid, direct, quantitative, and label-free detector of cardiac biomarker troponin T using near-infrared fluorescent single-walled carbon nanotube sensors. *Adv Healthc Mater* 3(3):412–423.
- Salem DP, et al. (2016) Chirality dependent corona phase molecular recognition of DNA-wrapped carbon nanotubes. *Carbon* 97:147–153.
- Kruss S, et al. (2014) Neurotransmitter detection using corona phase molecular recognition on fluorescent single-walled carbon nanotube sensors. *J Am Chem Soc* 136(2):713–724.
- Cragg SJ, Rice ME (2004) DANCING past the DAT at a DA synapse. *Trends Neurosci* 27(5):270–277.
- Wise RA (2004) Dopamine, learning and motivation. *Nat Rev Neurosci* 5(6):483–494.
- Hires SA, Zhu Y, Tsien RY (2008) Optical measurement of synaptic glutamate spillover and reuptake by linker optimized glutamate-sensitive fluorescent reporters. *Proc Natl Acad Sci USA* 105(11):4411–4416.
- Garris PA, Ciolkowski EL, Pastore P, Wightman RM (1994) Efflux of dopamine from the synaptic cleft in the nucleus accumbens of the rat brain. *J Neurosci* 14(10):6084–6093.
- Liang R, Broussard GJ, Tian L (2015) Imaging chemical neurotransmission with genetically encoded fluorescent sensors. *ACS Chem Neurosci* 6(1):84–93.
- Masharina A, Raymond L, Maurel D, Umezawa K, Johnson K (2012) A fluorescent sensor for GABA and synthetic GABA(B) receptor ligands. *J Am Chem Soc* 134(46):19026–19034.
- Bucher ES, Wightman RM (2015) Electrochemical analysis of neurotransmitters. *Annu Rev Anal Chem (Palo Alto, Calif)* 8(1):239–261.
- Adams KL, Puchades M, Ewing AG (2008) In vitro electrochemistry of biological systems. *Annu Rev Anal Chem (Palo Alto, Calif)* 1:329.
- Omiatsek DM, Cans AS, Heien ML, Ewing AG (2010) Analytical approaches to investigate transmitter content and release from single secretory vesicles. *Anal Bioanal Chem* 397(8):3269–3279.
- Keighron JD, Ewing AG, Cans AS (2012) Analytical tools to monitor exocytosis: A focus on new fluorescent probes and methods. *Analyst (Lond)* 137(8):1755–1763.
- Gubernator NG, et al. (2009) Fluorescent false neurotransmitters visualize dopamine release from individual presynaptic terminals. *Science* 324(5933):1441–1444.
- Zhang J, et al. (2013) Molecular recognition using corona phase complexes made of synthetic polymers adsorbed on carbon nanotubes. *Nat Nanotechnol* 8(12):959–968.
- Bisker G, et al. (2016) Protein-targeted corona phase molecular recognition. *Nat Commun* 7:10241.
- Bisker G, et al. (2015) A mathematical formulation and solution of the CoPhMoRe inverse problem for helically wrapping polymer corona phases on cylindrical substrates. *J Phys Chem C* 119(24):13876–13886.
- Polo E, Kruss S (2016) Impact of redox-active molecules on the fluorescence of polymer-wrapped carbon nanotubes. *J Phys Chem C* 120(5):3061–3070.
- Kruss S, Srot V, van Aken PA, Spatz JP (2012) Au-Ag hybrid nanoparticle patterns of tunable size and density on glass and polymeric supports. *Langmuir* 28(2):1562–1568.
- Kruss S, et al. (2013) Adhesion maturation of neutrophils on nanoscopically presented platelet glycoprotein Iba. *ACS Nano* 7(11):9984–9996.
- Kruss S, et al. (2010) Stimulation of cell adhesion at nanostructured teflon interfaces. *Adv Mater* 22(48):5499–5506.
- Greene LA, Tischler AS (1976) Establishment of a noradrenergic clonal line of rat adrenal pheochromocytoma cells which respond to nerve growth factor. *Proc Natl Acad Sci USA* 73(7):2424–2428.
- Westerink RH, Ewing AG (2008) The PC12 cell as model for neurosecretion. *Acta Physiol (Oxf)* 192(2):273–285.
- Attiah DG, Kopher RA, Desai TA (2003) Characterization of PC12 cell proliferation and differentiation-stimulated by ECM adhesion proteins and neurotrophic factors. *J Mater Sci Mater Med* 14(11):1005–1009.
- Cho Y, Borgens RB (2010) The effect of an electrically conductive carbon nanotube/collagen composite on neurite outgrowth of PC12 cells. *J Biomed Mater Res A* 95(2):510–517.
- Leach JB, Brown XQ, Jacot JG, Dimilla PA, Wong JY (2007) Neurite outgrowth and branching of PC12 cells on very soft substrates sharply decreases below a threshold of substrate rigidity. *J Neural Eng* 4(2):26–34.
- Sudibya HG, et al. (2009) Interfacing glycosylated carbon-nanotube-network devices with living cells to detect dynamic secretion of biomolecules. *Angew Chem Int Ed Engl* 48(15):2723–2726.
- Rodriguez PC, et al. (2013) Fluorescent dopamine tracer resolves individual dopaminergic synapses and their activity in the brain. *Proc Natl Acad Sci USA* 110(3):870–875.
- Byrd JC, Hadjiconstantinou M, Cavalla D (1986) Epinephrine synthesis in the PC12 pheochromocytoma cell line. *Eur J Pharmacol* 127(1-2):139–142.
- Kumar GK, et al. (1998) Release of dopamine and norepinephrine by hypoxia from PC-12 cells. *Am J Physiol* 274(6 Pt 1):C1592–C1600.
- Zerby SE, Ewing AG (1996) Electrochemical monitoring of individual exocytotic events from the varicosities of differentiated PC12 cells. *Brain Res* 712(1):1–10.
- Schroeder TJ, Jankowski JA, Senyshyn J, Holz RW, Wightman RM (1994) Zones of exocytotic release on bovine adrenal medullary cells in culture. *J Biol Chem* 269(25):17215–17220.
- Hirasawa H, Contini M, Raviola E (2015) Extrasynaptic release of GABA and dopamine by retinal dopaminergic neurons. *Phil Trans R Soc London Biol Sci* 370(1672):20140186.
- Martens S, McMahon HT (2008) Mechanisms of membrane fusion: disparate players and common principles. *Nat Rev Mol Cell Biol* 9(7):543–556.
- Zhao WD, et al. (2016) Hemi-fused structure mediates and controls fusion and fission in live cells. *Nature* 534(7608):548–552.
- Becherer U, et al. (2007) Quantifying exocytosis by combination of membrane capacitance measurements and total internal reflection fluorescence microscopy in chromaffin cells. *PLoS One* 2(6):e505.
- Amatore C, Arbault S, Lemaître F, Verchier Y (2007) Comparison of apex and bottom secretion efficiency at chromaffin cells as measured by amperometry. *Biophys Chem* 127(3):165–171.
- Belyaev AG (1999) A note on invariant three-point curvature approximations. *RIMS* 1111:157–164.